In-situ monitoring of a PVT-heat pump system with ground sources used for heating and cooling applications

Krishna Prasad Timilsina, Bharat Chhugani and Peter Pärisch

Institute for Solar Energy Research Hamelin (ISFH), Germany

Abstract

Photovoltaic-thermal (PVT) collectors are regarded as a potential key technology for climate-neutral energy supply in buildings due to their feature of cogenerating thermal and electrical energy. This paper analyses the performance of a demo plant consisting of uncovered (WISC) PVT collectors in a system configuration, with a brine-to-water heat pump and ground sources i.e., borehole and horizontal ground heat exchangers, used for heating and cooling purposes in a non-residential building. The seasonal performance factor of the system before storage (SPF_{bSt}) for the monitored year 2022 was 3.3 in the heating mode and 4.1 in the cooling mode. PVT collectors proved to be an essential source in the system, covering around a quarter of the heating demands and around 35 % of the cooling demands through nocturnal cooling. In addition, 56 % of the solar heat produced by PVT collectors was used for the regeneration of the ground sources. In this demo site, the solar regeneration enabled the sizing of relatively smaller ground sources during the design phase. Furthermore, the thermal parameters of the PVT collectors are identified with the monitoring data according to the quasi-dynamic test (QDT) mathematical model based on ISO 9806. On average, the typical heat loss coefficient defined specifically for nocturnal cooling per m² PVT estimated from the monitoring data was 21 W/K.

Keywords: PVT collectors, heat pump, monitoring, heating, cooling, quasi-dynamic test method, thermal parameters

1. Introduction

A major challenge for the shift from conventional to renewable energy sources is the transition of heating and cooling systems in buildings to renewables. In 2021, renewables accounted for only 22.9 % of European heating and cooling consumption, and natural gas alone covered 34.3 % of the continent's heating demand (Eurostat 2023). In Germany, only 15.4 % of the energy consumed for heating and cooling of buildings came from renewable sources in 2021 which increased to 17.4 % in 2022 (Umwelt Bundesamt, 2023). Due to the high dependence on natural gas and its imminent insecurity of supply, there is an urgent need for Western European nations to explore alternative solutions for heat supply (Eurostat 2023). As one of the main CO_2 emitters, the building sector must be efficiently integrated with renewable energy technologies to meet the emission targets. In this context, research and applications of solar photovoltaic-thermal (PVT) collectors have significantly increased due to their benefits of gaining electrical and thermal yields from the same aperture area. Therefore, PVT collector-based heat pump systems are considered to play a pivotal role in achieving the emission and energy efficiency targets in building sectors. In 2022, the uncovered PVT collectors had 87 % of the market share due to relatively favourable subsidy schemes (Weiss and Spörk-Dür, 2023). Due to the convective and radiative heat transfer potential of the uncovered PVT collectors, they can also be used for passive cooling of buildings during the night. In order to analyse the performance and efficiency of the installed systems, they need to be monitored under real operating conditions.

This paper is based on the results of the ongoing project “integraTE”, which focuses on PVT systems and aims to increase market penetration of technically and economically attractive energy supply through PVT collector-heat pump systems in the building sector. One of the work packages of the project is the monitoring of 10 demo plants consisting of PVT as a single or additional heat source for the heat pump. The case study presented in this paper is focused on a non-residential building, serving as one of the demo plants, wherein a heat pump system is employed to fulfil both heating and cooling requirements. The main aim of this study is to evaluate the heat pump and system efficiency and to analyse the performance of PVT collectors under various operating

10.18086/swc.2023.04.02 Available at http://proceedings.ises.org

and environmental conditions. Furthermore, the thermal performance parameters of the PVT collectors based on ISO 9806:2013 (ISO 9806, 2013) have also been calculated from the monitoring data and compared with the parameters obtained from the laboratory tests conducted as defined in the standard.

2. System Description

Fig 1 illustrates the simplified schematic layout of the monitored system. The solid lines in the figure represent the flow pipes and the broken lines indicate the return pipes. The orange coloured lines indicate pipes transporting fluid with lower temperatures i.e. at heat pump sources or cooling circuits. Conversely, the red lines denote the pipes carrying fluid with higher temperatures i.e. sink side of the heat pump. The fluid flowing in the lines prior to the heat exchanger (HEX) depicted in the diagram is a mixture of brine and water, whereas the green lines beyond the heat exchanger represent the water-based heating and cooling circuits. The system comprises uncovered PVT collectors, borehole heat exchangers (BHE) and horizontal ground heat exchangers (HGHE) serving as sources for a brine-to-water heat pump. The description of these components is shown in Tab 1.

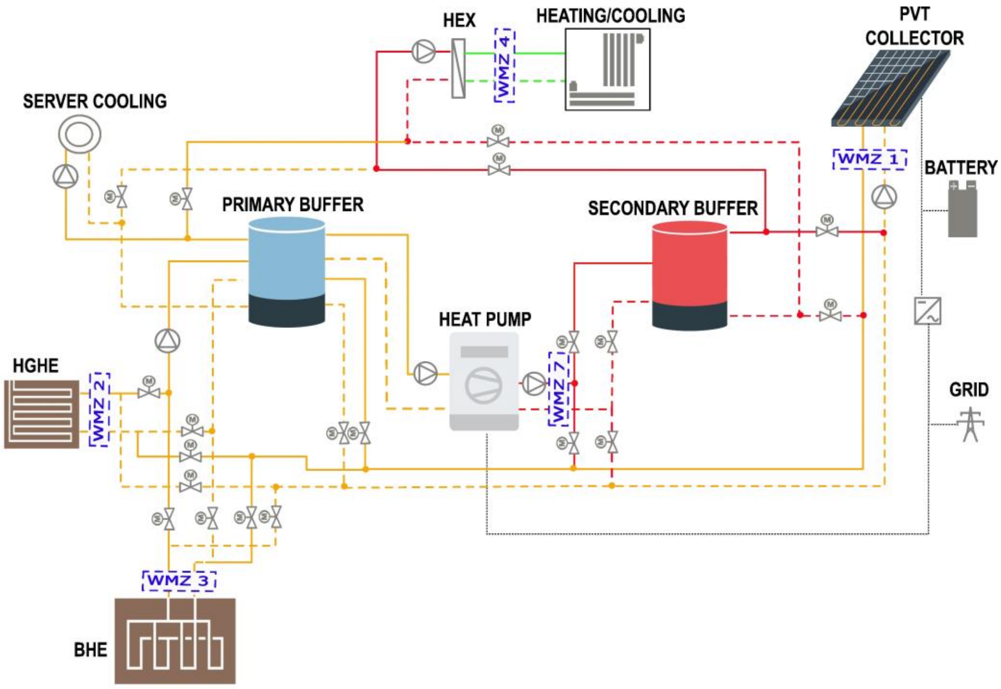

Fig. 1: Simplified hydraulic schematic diagram of the monitored system

Tab. 1: Description of heat sources and heat pump

PVT modules type	Uncovered (WISC) with aluminium heat exchanger on the rear side, see Fig. 2(b)
PVT collectors (thermal)	Area: 230 m²
PV electrical capacity (PV+PVT)	Type: Monocrystalline PV Area: 325 m^2 Power: 61 kWp
Heat pump	Type: Brine-water (B0/W35) Heating capacity: 58.6 kW Cooling capacity: 46.3 kW COP: 4.8
Borehole heat exchangers	6 x boreholes à 100 m depth
Horizontal ground heat exchangers	Area: 360 m^2 (two layers)

The storage system consists of two buffer tanks each 3000 l, one on the source side of the heat pump (primary buffer) and the other on its sink side (secondary buffer). The secondary buffer serves as a distribution tank for the heat supply whereas the primary buffer supplies the heat provided by PVT collectors, BHE and HGHE to the heat pump. Additionally, the primary buffer operates as a distribution tank for server and space cooling of the buildings. The demo plant consists of four buildings: the main building (i.e. office building) and three ancillary buildings, which are used as seminar rooms and for exhibitions or external events. The distribution system delivers the heat from secondary buffer storage to all the aforementioned buildings through a brazed plate heat exchanger (HEX in Fig. 1). The designed supply and return temperatures to the heat exchanger for heating mode are 47 °C and 42 °C respectively. Similarly, for the cooling mode, the respective design supply and return temperatures are 14 °C and 19 °C. The electricity produced by the PV modules is either supplied to the heat pump, fed to the grid or used to charge the batteries and supply electricity to the buildings.

Further information on the system is listed below:

- Location of project: Hannover, Germany
- Year of construction/renovation: 1999 / 2020
- Heated living area: 1803 m^2
- Building heating/cooling load: 58.6 kW / 54 kW
- Method of heating: radiator, floor heating, convectors
- Simulated yearly heat demand: 84,907 kWh
- Simulated yearly cooling demand: 47,694 kWh

3. Monitoring

The monitoring system is equipped with devices and sensors for measuring weather conditions, and the heat and electricity consumed or produced within the system. Each device and sensor independently exports event-driven data to the database i.e. the data is logged exclusively when there is a change in specific sensor readings. Therefore, each sensor has its own time-series data, which has to be merged before analysis.

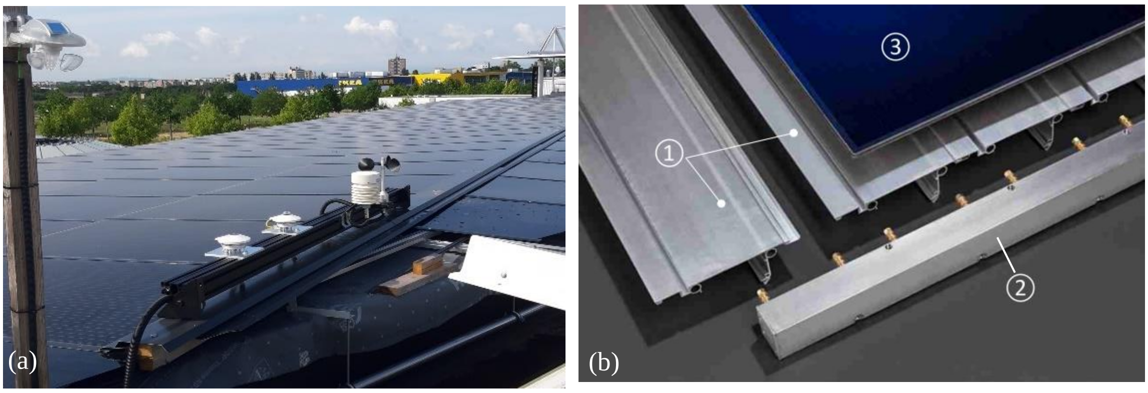

Fig. 2:(a) Weather station installed at PV-PVT field and (b) PVT-module (1. Extruded aluminium profiles, 2. Manifold, 3. PV-module)

Fig. 2(a) shows the weather station installed at the PVT collector field on the roof of the main building. It consists of a transmitter with PT100 temperature sensors and humidity sensors to measure ambient temperature and relative humidity. Additionally, it incorporates a pyranometer to measure solar irradiance, a pyrgeometer to measure longwave irradiance and a wind transmitter to measure wind speed. A total of seven bidirectional heat flow meters are installed to monitor the heat flow at PVT, HGHE, BHE, heat pump condenser and distribution circuits. The heat flow meters installed in the brine loops, i.e. PVT collector, BHE, HGHE and heat pump sink side are based on ultrasonic volume flow sensors and PT500 temperature sensors for flow and return temperatures. Three heat flow meters in the distribution systems based on ultrasonic volume flow sensors and PT100 temperature sensors are installed to record the flow and return temperature of the heating/cooling circuits of three different buildings. The positions of the five main heat flow meters used to create the energy balance of the system are shown in Fig. 1 as “WMZ”. An electricity meter monitors the total electricity consumption of the heat pump, including the circulation pumps on the source and sink sides. Also, the electricity generated from both the PVT collectors and the PV modules is recorded at three different inverters. The electricity consumed by the circulation pumps for the ground sources and the PVT collectors is also recorded. Three PT1000 temperature sensors are used to monitor the temperature of the ground at different depths (5 m, 25 m, and 50 m) for BHE and a temperature sensor records the temperature of the HGHE field at 1.5 m depth.

4. Operation Modes

In the data, an operation mode is assigned to each instance (1 minute) based on the operation status (on/off) of heat sources, heat sinks and the heat pump. The energy flow at any instance is determined based on the operation mode active at that particular occasion. As shown in Fig. 3(left), in heating operation modes, heat sources like PVT, BHE and HGHE supply heat to the primary buffer storage, which is finally delivered to the heat pump evaporator based on the heating requirement at the secondary buffer. The heat pump condenser supplies heat to charge the secondary buffer storage tank which acts as a distribution tank for supplying heat to the buildings. Additionally, in regeneration modes, solar heat from PVT collectors is stored in either BHE or HGHE.

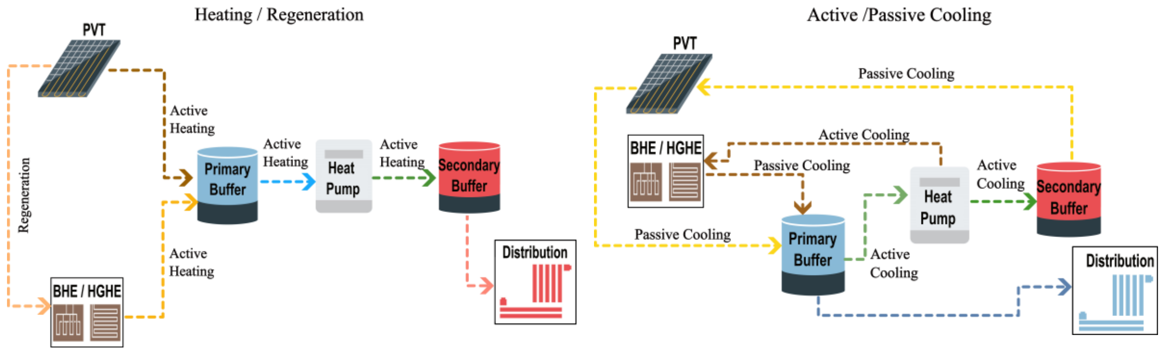

Fig. 3: Operation modes of the system

As shown in Fig. 3(right) cooling modes are divided into active and passive cooling based on the use of the heat pump during cooling operation. Active cooling refers to the cooling modes where the primary buffer storage is cooled through the evaporator of the heat pump where the heat from primary buffer storage is transferred either to the secondary buffer storage or to the ground sources. On the other hand, passive cooling refers to cooling operations without heat pump usage. During passive cooling with BHE and HGHE, the primary buffer is cooled with the aid of circulation pumps when the ground temperatures are on sufficiently lower levels. The PVT collectors cool the secondary buffer through nocturnal passive cooling in summer.

The reference temperatures are compared to enable each operating mode. If the regulatory conditions are met, the operating mode is activated. The system chooses the operation modes according to the following priority order: passive cooling, active cooling, active heating and secondary buffer cooling/regeneration. This priority order is used to decide which mode should be active at a certain instance. The heat pump controller receives a heating or cooling request from the higher-level control. Depending on the requirement, the heat pump monitors primary or secondary storage tanks and keeps them within the defined temperature limits.

5. KPIs for heat pump and system efficiency

To determine the efficiency of the heat pump and the system for heating and cooling modes separately, seasonal performance factors (SPF) for various system boundaries are defined. The SPF is the indicator of the efficiency of the system over a season (or a year). It is the ratio of the useful thermal energy (heating or cooling) supplied by the system to the electrical energy used by the system. Therefore, the SPF of the system during cooling operation differs from that of heating as the useful energy in the cooling mode is obtained from the source side of the heat pump. For the monitored system, the $SPF_{bSt,H}$ as specified in eq. 1 is the ratio of the amounts of heat supplied to the secondary buffer by the heat pump ($\dot{Q}_{HP}$), divided by the electrical energy consumed within the boundary i.e. before storage (Malenković et al., 2013). The electrical power consumed by the heat pump compressor as well as the internal circulation pumps and controls is denoted by $\dot{E}_{HP}$ and $\dot{E}_{Pumps}$ is the electricity consumed by circulation pumps for ground sources and PVT collectors within the system boundary.

Eq. 2 is used to calculate the seasonal performance factor for cooling $SPF_{bSt,C}$ which is the ratio of the total cooling energy delivered to the primary buffer, to the associated electricity consumption (Gehlin and Spitler, 2022; Malenković et al., 2013). The cooling energy delivered to the primary buffer from the heat pump evaporator during active cooling modes is denoted by $\dot{Q}_{Evap}$, and $\dot{Q}_{Passive}$ indicates the heat removed from the primary buffer by HGHE, BHE and PVT without the heat pump operation through passive cooling. To determine the efficiency of the heat pump over a certain period, the coefficient of performance $SPF_{HP,H}$ given in eq. 3 is used, which relates the corresponding integrated amounts of heat supplied, and electricity consumed. Accordingly, eq. 4 is used to calculate the heat pump's coefficient of performance during active cooling i.e. $SPF_{HP,C}$.

$$SPF_{bSt,H} = \frac{\int \dot{Q}_{HP}\, dt}{\int (\dot{E}_{HP} + \dot{E}_{Pumps})\, dt} \quad \text{(eq. 1)}$$

$$SPF_{bSt,C} = \frac{\int (\dot{Q}_{Evap} + \dot{Q}_{Passive})\, dt}{\int (\dot{E}_{HP} + \dot{E}_{Pumps})\, dt} \quad \text{(eq. 2)}$$

$$SPF_{HP,H} = \frac{\int \dot{Q}_{HP}\, dt}{\int \dot{E}_{HP}\, dt} \quad \text{(eq. 3)}$$

$$SPF_{HP,C} = \frac{\int \dot{Q}_{Evap}\, dt}{\int \dot{E}_{HP}\, dt} \quad \text{(eq. 4)}$$

6. Results

6.1. Performance during heating modes

The complete monitoring of the system has been ongoing since January 2022 and all the findings presented in the work are based on the data collected in the year 2022. During the analysis of the system, a separate energy balance is established for heating and cooling modes. Fig. 4 shows the monthly energy balance and the performance factors (PF) during the heating operation. The energy quantities Q_{PVT}, Q_{BHE} and Q_{HGHE} denote the respective thermal energy contributions from the PVT collectors, BHE and HGHE to the heat pump evaporator. In 2022, the PVT collectors supplied 14,384 kWh of thermal energy to the primary buffer, which is about 24 % of the total heat accumulated in the primary buffer and utilized as a heat pump source. The major heat source for the heat pump system was the BHE field, contributing to 46 % of the total heat, while the HGHE field covered 8 % of the heat delivered to the primary buffer.

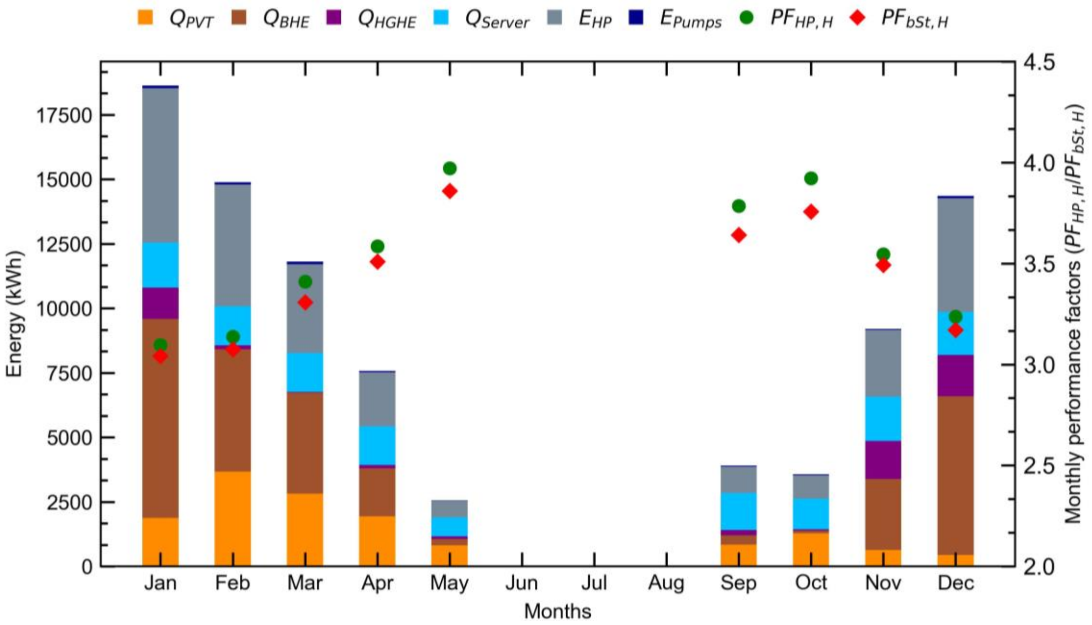

Fig. 4: Monthly energy balance and performance factor for heating modes of operation

The heat accumulated in the primary buffer due to server cooling is also included in Fig. 4 as Q_{Server}. The amount of server cooling was determined from the difference in energy balance at the heat pump, as there is no heat flow meter installed in the server cooling circuit. Throughout the year, the heat gains through server cooling accounted for 22 % of the energy flowing into the primary buffer. During the heating season, the heat pump condenser delivered a cumulative thermal energy output of 85,935 kWh to the secondary buffer storage with a corresponding electricity consumption of 25,788 kWh. The seasonal performance factor of the heat pump $SPF_{HP,H}$ was 3.33. The electricity consumption of the circulation pumps on the source and sink side of the heat pump is measured together with the electricity consumption of the heat pump (E_{HP}). This could be one of the reasons for relatively lower $SPF_{HP,H}$ in the context of similarly configured systems. The annual heat supplied to the buildings via the heat exchanger in the distribution system amounted to 85,590 kWh, equivalent to 47.5 kWh/(m^2·a). This heat delivery matched very well the simulated annual heat demand determined by the planner with the tool TRNSYS, i.e. 84,909 kWh. The seasonal performance factor of the system before storage during heating periods i.e. $SPF_{bSt,H}$, for the year 2022 was 3.3. The circulation pump on the heat pump sink side was running during the heating periods due to a control fault, although the heat pump was not operating. This resulted in increased electricity consumption and could be one of the reasons for the lower system efficiency during heating periods. The simultaneous heating and cooling with multiple sources and the complexity of the system make it difficult to identify the specific reason for the lower system efficiency.

6.2. Performance during Cooling

Fig. 5(a) presents the monthly performance factors and energy balance observed at the heat pump condenser during the active cooling of the primary buffer (cold storage). From mid-May to the end of August 2022, the system was solely used for cooling. The seasonal performance factor of the heat pump in cooling mode ($SPF_{HP,C}$) was 4.08. When including cooling gains through passive cooling and the electrical consumption of the circulation pumps, $SPF_{bSt,C}$ resulted to 4.14. Due to the inclusion of passive cooling of the primary buffer through BHE and HGHE, the $SPF_{bSt,C}$ is slightly higher than the heat pump's coefficient of performance. The higher performance factors observed during active cooling (compared to the heating modes) can be attributed to the lower supply temperatures of the heat pump (see Fig. 5(b)). During the active cooling mode, 17,819 kWh of heat was extracted from the primary buffer from May to October. The excess heat from the primary buffer was transferred through the heat pump condenser either to the ground ($Q_{BHE,reg}$, $Q_{HGHE,reg}$) or to the secondary buffer, which is then cooled by the PVT collectors through passive night cooling ($Q_{PVT,C}$). A total of 13,552 kWh of heat was injected into the ground during active cooling operation (approx. 95 % to the BHE field and 5 % to the HGHE field). In addition, only 377 kWh of heat from the cold storage was fed into the ground through passive cooling of the primary buffer. In total, 35 % of the heat in the primary buffer is dissipated by the PVT collectors and the remaining 65 % by the ground sources (BHE and HGHE). The waste heat during active cooling with ground sources accounted for around 44 % of the heat injected into the ground.

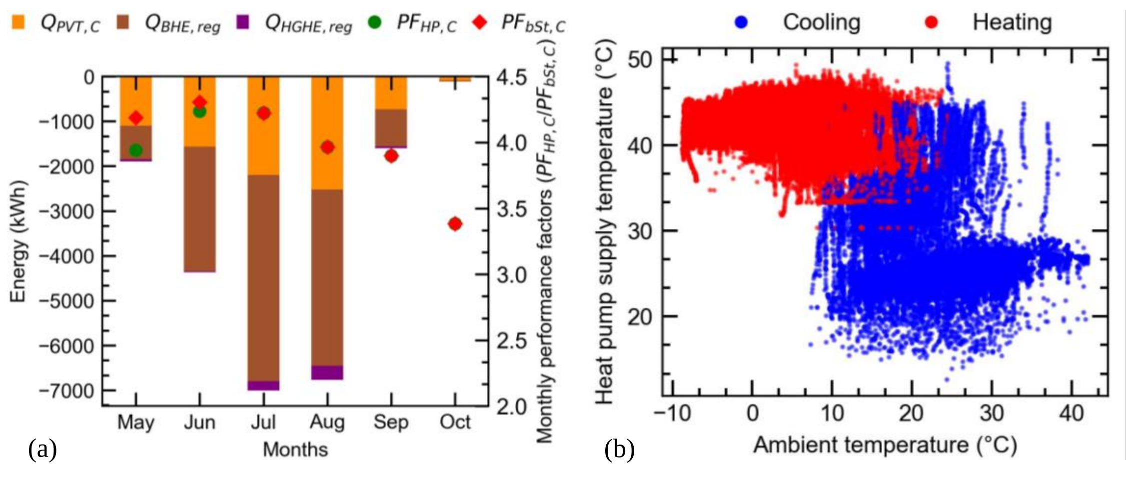

Fig. 5: (a) Monthly energy balance and performance factors during cooling modes (b) Heat pump supply temperature as a function of ambient temperature (minute resolution)

Fig. 5(b) illustrates two distinct supply temperature ranges observed during the heat pump's operation. The data points with the supply temperatures between 35 °C and 48 °C (red cluster) represent the instances when the heat pump is used for heating. The other instances when the heat pump supply temperatures range from

15 °C to 45 °C (blue cluster) refer to the active cooling modes. Upon closer analysis, it was found that most of the concentrated points between 18 to 28 °C refer to active cooling with the ground sources. The remaining points refer to active cooling with the secondary buffer i.e. the instances where the secondary buffer is charged with the excess heat from the primary buffer. At the end of a typical summer day with cooling demands, the secondary buffer ends the day warm with temperatures up to 45 °C and at night, the PVT collectors cool it to temperatures as low as 15 °C. The ambient temperature during heating varied from -8 °C to 25 °C. And during cooling, the ambient temperature was between 10 °C to 42 °C. During higher ambient temperatures, particularly during summer days, the waste heat was directed to the ground as buffer cooling with PVT collectors is not possible for operating conditions with an inlet temperature lower than the ambient temperature. The higher values of the ambient temperatures could be due to the installation of the temperature sensors on the PVT field.

6.3. Energy balance at PVT collectors

Fig. 6 displays the comprehensive overview of monthly thermal energy supplied by the PVT collectors for heating ($Q_{PVT,HP}$), regeneration ($Q_{Regeneration}$) and cooling ($Q_{Nightcooling}$). The thermal yield of the PVT collectors increased from 1,946 kWh in January to 8,461 kWh in April. Despite the PVT collectors' inherent capacity to capture more solar thermal energy during summer months, the actual positive thermal yield remained relatively low due to simultaneous cooling requirements and no heat demand, i.e. domestic hot water preparation. From mid-May to the end of August, the PVT collectors were only used for cooling, releasing 8,404 kWh of heat from the secondary buffer to the surrounding environment via passive nocturnal cooling. Also, in September, the PVT collectors released 701 kWh of heat to the ambient air in addition to the heating and regeneration. The regeneration of the ground with PVT collectors increased from 30 kWh in January to 6,517 kWh in April. To sustain lower ground temperatures essential for cooling, the solar regeneration was intentionally halted from mid-May to the end of August. The ground regeneration restarted at the end of August with the end of the cooling season. In 2022, a total of 56 % of the solar heat was used for ground regeneration. Approximately, 70 % of this energy was injected into the BHE field and the remaining 30 % into the HGHE field. According to the planner, this advantage of regeneration through PVT collectors allowed the planning of shorter borehole lengths. Furthermore, combining PVT with ground sources in this type of system also helps to prevent dropping ground temperatures in the long term.

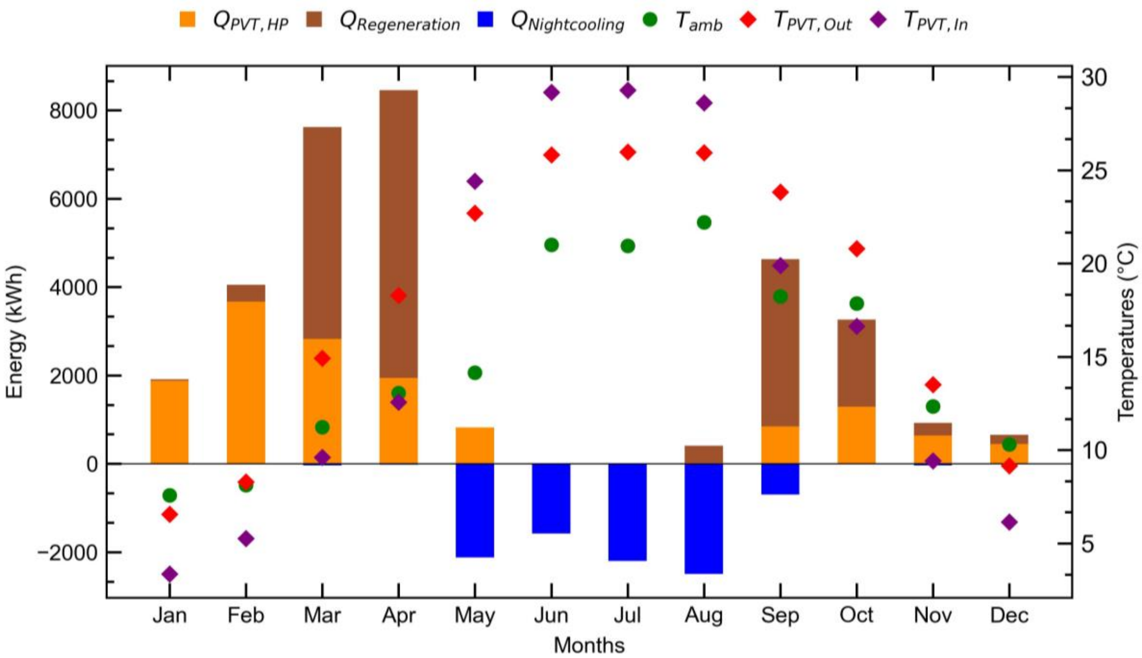

Fig. 6: PVT energy balance and system temperatures

In addition, Fig. 6 illustrates the comparison of the monthly average inlet and outlet temperatures of the PVT collector field ($T_{PVT,In}$ and $T_{PVT,Out}$) and the ambient temperature (T_{amb}). During the winter months (i.e. November to February) which correspond to the heating period, the outlet temperatures are on average 3.2 K higher than the inlet temperature. During the regeneration periods, i.e. in March and April, the difference is relatively higher, with an average of 5.5 K. In the summer months (i.e. May to August), when the PVT collectors were primarily used for passive night cooling to cool the secondary buffer, the inlet temperatures are on average 2.8 K higher than the outlet temperatures. From September onwards, the PVT collectors are used again for heating and regeneration, with an average temperature difference of 3.8 K. In winter and transition seasons, when the ambient temperatures were higher than the inlet temperatures, the PVT collectors gained additional heat from the environment. These observations highlight the dynamic temperature variations and seasonal performance of the PVT collector system.

Fig. 7(a) shows ambient temperature as a function of the sky temperature during the cooling modes using PVT collectors. The sky temperature was indirectly calculated using the longwave irradiance measured by a pyrgeometer. The temperature difference between the ambient air and the sky during these instances was up to 20 K with an average of 11 K. Due to higher fluid temperatures coming from the secondary buffer storage and relatively lower ambient and sky temperature conditions, the night radiative cooling potential of PVT collectors during cooling mode is significant.

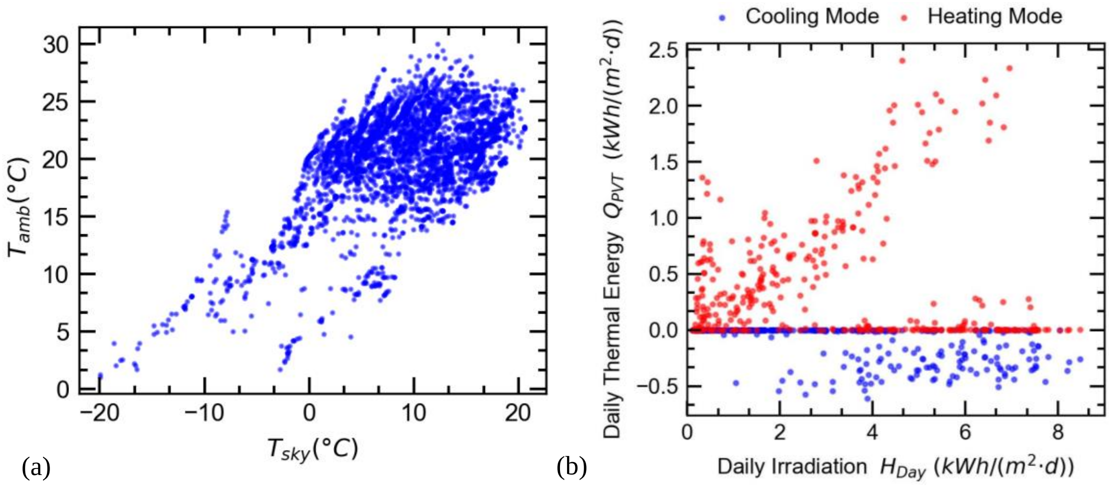

Fig. 7: (a) Sky temperature vs. ambient temperature during cooling with PVT collectors (5-minute resolution); (b) Daily thermal energy as a function of irradiation

6.4. Irradiation and thermal energy yield of PVT collectors

Fig. 7(b) shows the daily heating (positive) and cooling (negative) thermal energies of the PVT collectors compared to the total daily irradiation. The graph indicates that despite a substantial daily solar irradiance of more than 2 kWh/(m^2·d), there were numerous days when the positive thermal energy of the PVT collectors was zero or close to zero. This occurred due to one of two scenarios: either the collectors were not operational on these days or were exclusively used for cooling. The blue dots with negative thermal energy represent the days when collectors were used for passive night cooling of the secondary buffer. The significant observation here is the presence of positive thermal energy of up to 1.4 kWh/(m^2·d) at lower solar irradiation (below 1 kWh/(m^2·d)). This phenomenon underlines the PVT collector's ability to extract thermal energy from the surrounding air, effectively functioning as an environmental heat exchanger when the ambient temperatures are higher than the inlet temperature of the collectors. This capability is attributed to the fact that the rear side of the collector is exposed to the external environment, as illustrated in Fig. 2(b). To determine how efficiently the PVT collectors, convert the incident irradiance into energy, the utilization rate is calculated for both the thermal and the electrical parts. The solar thermal utilization rate is defined as the ratio of the generated energy (heat) to the available energy (irradiation). With solar irradiation of greater than 1 kWh/(m^2·d), the solar thermal utilization rate of the PVT collector ranged from 23 % to 70 % with an average of approx. 40 %. Determination of the utilization rate is not plausible for lower irradiation levels, as the heat is not solely derived from irradiation but also absorbed from the surrounding environment, making the calculation less straightforward.

The annual specific heat yield of the PVT collectors was 152 kWh/(m^2·a). In addition, the specific annual cooling energy yield of PVT collectors was 40 kWh/(m^2·a). The use of geothermal sources for cooling in summer limited the permissible increase in ground temperatures, which restricted the regeneration potential of PVT collectors. For this reason, PVT collectors were not used on warm and sunny summer days, which significantly lowered the annual heat yield. In previous investigations involving systems configured for energy supply in single-family houses, which incorporated PVT and BHE as heat sources for heat pumps, comparatively higher thermal energy yields ranging from 330 to 450 kWh/(m²·a) were reported (Helmling et al., 2022). Furthermore, in a non-residential building investigated in a project in Switzerland, the heat yield was 440 kWh/(m²·a) (Zenhäusern et al., 2017). The reason for the higher heat yields of the PVT collectors in these systems compared to the system investigated in this paper is that the PVT collectors were additionally used for hot water production and regeneration of the ground in summer.

6.5. PVT-Collector thermal performance parameters based on ISO 9806

The standard thermal performance parameters calculated using the quasi-dynamic test (QDT) method based on ISO 9806 (2013) are already available for the PVT collector discussed in this paper (Brötje et al., 2018). However, it is important to note that these parameters may vary under real operation due to the different installation, operating and environmental conditions. In our specific case, the test parameters do not reflect the collector's operation without solar irradiance for heating the primary buffer as well as its use during summer nights for cooling. The goal of the work was to determine the PVT collector parameters using yearly data from in-situ monitoring and to evaluate the performance of the PVT collectors under real conditions, installed on a flat roof with a substructure.

The data was first resampled to a five-minute interval as the collector field was large and averaging the data would better characterize the inlet and outlet temperature of the collector field. Valid data points were then selected to characterize the transient behaviour of the PVT collectors by eliminating probable outliers. According to the QDT mathematical model based on ISO 9806 given in eq. 5, the coefficients were determined using robust nonlinear least-squares fitting in Python, but considering both daytime and nighttime data. The older version of ISO 9806 was used to enable comparison of the parameters obtained from the monitoring data with the existing parameters from collector testing. The uncertainty of measurements was not considered in the calculations.

$$\dot{q}_{th} = \boldsymbol{\eta_{0,hem}} \cdot G_{hem} - \boldsymbol{c_1} \cdot (\vartheta_m - \vartheta_a) - \boldsymbol{c_2} \cdot (\vartheta_m - \vartheta_a)^2 - \boldsymbol{c_3} \cdot u \cdot (\vartheta_m - \vartheta_a) + \boldsymbol{c_4} \cdot (E_L - \sigma T_a^4) - \boldsymbol{c_5} \cdot \frac{d\vartheta_m}{dt} - \boldsymbol{c_6} \cdot u \cdot G_{hem} \quad \text{(eq. 5)}$$

$$c_4 = \eta_{0,hem} \cdot \frac{\varepsilon}{\alpha} \quad \text{(eq. 6)}$$

$$c_6 = \eta_{0,hem} \cdot b_u \quad \text{(eq. 7)}$$

The standard QDT model needed to be modified as shown in eq. 5 since the direct and diffuse radiation were not measured separately and only the global hemispherical irradiance (G_{hem}) was available for the monitoring data. The terms $\eta_{0,b} \cdot K_b(\theta) \cdot G_b + \eta_{0,b} \cdot K_d \cdot G_d$ in the standard QDT model are therefore replaced by $\eta_{0,hem} \cdot G_{hem}$ with the consideration that the IAMs (Incidence Angle Modifiers) K_d and K_d are one. To apply this modification, only incidence angles below 60° were applied for the calculation of the zero-loss efficiency $\eta_{0,hem}$. The collector parameters are identified iteratively in two steps. In the first step, the initial guess of $\eta_{0,hem}$ is kept constant and all the other parameters are calculated. In the second step, the parameters calculated in the first step are kept constant and the data with incidence angles below 60° is used to calculate the $\eta_{0,hem}$. In the next iteration, the calculated $\eta_{0,hem}$ is used as an updated constant for the first step and the iterations continue until the optimized parameters are obtained. To reduce the correlation between the parameters $\eta_{0,hem}$, c_4 and c_6, the relationships given in eq. 6 and eq. 7 are used based on the literature (Brötje et al., 2018). The parameter b_u refers to collector efficiency coefficient used to estimate wind dependence of zero-loss efficiency for uncovered collectors. The effective thermal capacity c_5 is kept constant as it is a material property and it is very complex to characterize it with the monitoring data. The parameter c_2 is also set to zero as it resulted in a negative value during the fitting and is also expected to be zero for these types of collectors. The statistical accuracy of the fitting is checked by the calculation of T-ratio as explained in ISO 9806 standard as the ratio of the resulting optimal value for the parameter to the standard error associated with the parameter fitting. The minimum T-ratio for each parameter to be accepted as statistically significant according to the standard is 3 and, in this case, the T-ratio for all the calculated parameters are greater than 35.

Tab. 2 shows a comparison between the collector coefficients obtained from monitoring data and the collector coefficients from the laboratory tests at ISFH. The heat loss coefficients, especially c_1 and c_3 exhibit the most substantial deviations compared to other parameters: the heat loss coefficient c_1 is 25 % lower and the wind dependence of heat loss coefficient c_3 is 18 % lower than the test results. The overall heat transfer coefficient (U-Value = c_1 + $c_3 \cdot u$), calculated for the wind speed of 1.3 m/s is 14.45 W/m²·K for the test parameters and 11.46 W/m²·K for the monitoring parameters i.e. 20 % lower for the monitoring parameters.

Tab. 2: PVT Collector thermal performance parameters according to ISO 9806:2013 for monitoring and test data

Parameter	Description	Monitoring	Test
$\eta_{0,hem}$	Peak collector (zero-loss) efficiency for total radiation (-)	0.66	0.62
c_1	Heat loss coefficient (W/m²·K)	9.64	12.24
c_2	Temperature dependence of heat loss coefficient (W/m²·K²)	0	0.06
c_3	Wind speed dependence of heat loss coefficient (J/m³·K)	1.40	1.7
c_4	Sky temperature (longwave radiation) dependence of heat loss coefficient	0.57	0.57
c_5	Effective thermal capacity (kJ/m²·K)	47.9	47.9
c_6	Wind speed dependence of the zero-loss efficiency (s/m)	0.04	0.03

During the tests at ISFH, the PVT field of 13.8 m² was installed parallel to a test roof with a 38° slope with the collector facing south. Whereas the collector field in the demo site is 17 times larger and installed on a horizontal roof with an inclination of 4.5° facing three different directions (east, south and north). The findings based on the previous investigations on the other PVT fields by Giovannetti et al. (2019) demonstrated the dependency of heat loss coefficients on installation conditions and the dimension of the field. Depending on the direction of the wind, a part of the PVT collector field could have higher exposure to wind than the other due to the inclination on a horizontal surface. However, this can only be confirmed with a detailed measurement of wind direction and wind speed at various positions of the collector field. Additionally, the different inclination of the collectors and the relatively smaller gaps between the substructure and the PVT-panels can obstruct active airflow on the rear side of the collector field, potentially contributing to the observed reduction in the U-value. The heat transfer on the rear side of the field is also less efficient compared to that in the laboratory tests. The zero-loss efficiency for total radiation is slightly higher compared to the test. The heat loss parameter c_6, is greater than the test values. The mass flow rate during the laboratory tests was between 40-53 kg/(m²·h), whereas the mass flow rate for the demo plant varied from 5-40 kg/(m²·h). The difference in mass flow rate and the mathematical model ($\eta_{0,hem}$ instead of $\eta_{0,b}$) could be the reason for the variation of the zero-loss coefficient and its wind dependence parameter.

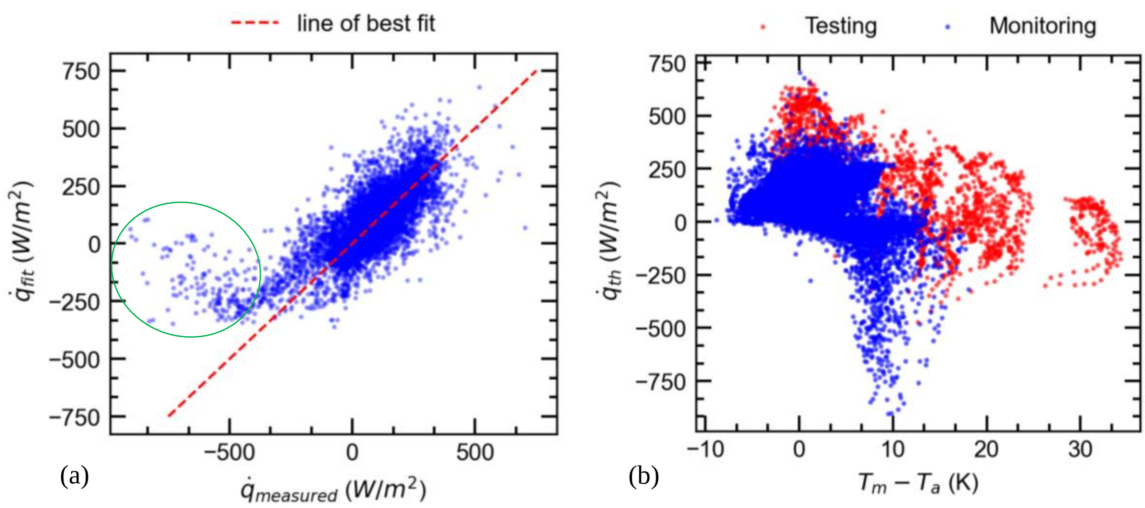

Fig. 8: (a) Comparison between measured and fitted specific thermal power of the PVT collectors for monitoring data, (b) Measured specific thermal power as a function of $T_m - T_a$ for testing and monitoring

Fig. 8(a) illustrates a reasonable fit between the measured and modelled specific thermal power for most instances. However, for $\dot{q}_{measured}$ below -500 W/m^2 (the cluster marked within the green boundary), the heat losses are underestimated. These data points correspond to the $\dot{q}_{th}$ below -500 W/m^2 denoted by blue dots in Fig. 8(b) and represent the data during the beginning of buffer cooling mode during summer nights. Compared to other operation modes, during these periods, the inlet temperature was higher (average of 31 °C), the average outlet temperature was 15 °C, ambient temperatures were moderate (average of 15 °C) and the average sky temperatures were 3.5 °C (minimum of -10 °C). These conditions indicate that the radiative heat losses dominate during those instances and higher values of c_4 can be expected. The use of eq. 6 for the calculation of c_4 could have led to an underestimation of the result as it is related to zero-loss efficiency. Our calculation shows that radiative heat losses accounted for at least 48 % of the total cooling achieved and the rest was covered by convective heat losses. However, these ratios serve as an initial approximation and could not be validated with the test results as the tests were not carried out during the night. Furthermore, to quantify the cooling potential of PVT collectors at night, the data during night cooling are considered to calculate a typical value for the heat loss coefficient. This typical heat loss coefficient, which is calculated as the ratio of measured specific thermal power ($\dot{q}_{th}$) and the temperature difference ($T_m - T_a$) for the night cooling, is 21 W/m^2·K. However, this value depends on and varies with ambient conditions like wind speed, ambient temperature and sky temperatures. In Fig. 8(b), the data points representing the test sequences with higher operating temperatures i.e. $T_m - T_a$ of more than 15 K up to 35 K (inlet temperatures up to 58 °C) do not exist in the monitoring data.

Tab. 2 shows the error estimates while calculating the collector thermal power using the two different parameter sets to fit the measured data. The column "Testing" refers to the error estimates calculated using the test parameters to estimate the fitted specific thermal power ($\dot{q}_{th,fit}$). Whereas the column "Monitoring" displays the corresponding error estimates based on the parameters identified from the monitoring data. Except for a very small deviation in RMSE, the error estimates show that the parameters obtained from the monitoring data provide comparatively better estimates for the specific thermal power ($\dot{q}_{th,fit}$). So, we can conclude that for the monitoring data, the identified parameters provide better accuracy.

Tab. 3: Comparison of accuracy of collector coefficients from testing and monitoring

Error Estimate	Equation	Testing	Monitoring
Root Mean Squared Error (RMSE)	$\sqrt{\frac{1}{N}\sum_{i=1}^{N}\left(\dot{q}_{th,measured} - \dot{q}_{th,fit}\right)^2}$	80.5 W/m^2	80.9 W/m^2
Mean Absolute Error (MAE)	$\frac{1}{N}\sum_{i=1}^{N}\left\lvert\dot{q}_{th,measured} - \dot{q}_{th,fit}\right\rvert$	51 W/m^2	48 W/m^2
R-Squared (R^2)	$1 - \frac{\sum_{i=1}^{N}\left(\dot{q}_{th,measured} - \dot{q}_{th,fit}\right)^2}{\sum_{i=1}^{N}\left(\dot{q}_{th,measured} - \dot{q}_{th,measured,Mean}\right)^2}$	0.52	0.59

7. Conclusions

This paper presents a case study of a PVT-heat pump system for heating and cooling operations in a non-residential building, with an emphasis on the thermal performance of PVT collectors. The system exhibited a moderate level of efficiency compared to other systems with similar configurations studied within the same project. For the heating period, the seasonal performance factor $SPF_{bSt,H}$ was 3.3 and for the cooling period, $SPF_{bSt,C}$ was 4.1. The PVT collectors made a significant contribution to the system, supplying 24 % of the heat and 35 % of the cooling energy to the primary buffer. In particular, for commercial buildings with limited roof space, PVT collectors demonstrated the advantage of providing electricity, cooling and heating in the same area. Overall, PVT collectors proved to offer greater flexibility for geothermal heat pump systems supporting both heating and cooling operations, as well as regenerating the ground during transition seasons. However, in terms of efficiency, this system configuration appears to be relatively inefficient and additional analysis is required to further clarify the system performance.

In addition, the collector coefficients of the QDT model defined by ISO 9806:2013 were calculated using monitoring data and then compared with existing parameters from standardized tests. The deviation in parameters could be attributed to two main aspects: the difference in environment and installation conditions and the difference in operation mode. The new set of parameters provided a better fit to the QDT mathematical model. The inclusion of night data related to the passive cooling operation is particularly relevant for the uncovered (WISC) PVT collectors without rear-side insulation like the one described in this paper. However, there is currently no such standardized framework for the inclusion of such data during the parameter identification, which is very important for the representation of the performance of the WISC PVT collectors for operation in periods without solar irradiation. Therefore, the collector parameters obtained in this paper can be used to describe the performance of the specific PVT collectors for heating as well as cooling under real operating and installation conditions. However, they cannot be used to define the performance of the collectors under standard testing conditions and to compare them with the other PVT collectors. Standard test sequences for nighttime testing need to be defined for the identification of an additional parameter set that represents the performance of PVT collectors at night i.e. during night cooling and heat gains from the environment.

8. Acknowledgements

The presented work and the results are part of the research project “integraTE - 03EGB0023”, funded by the Federal Ministry of Economics and Climate Protection (BMWK) and the state of Lower Saxony and carried out with Fraunhofer-ISE and IGTE of Stuttgart University. Furthermore, we would like to thank our industry partners nD-System GmbH, Architektur- und TGA-Planungsbüro Carsten Grobe, PA-ID Prozess GmbH, TripleSolar BV, SunMaxx PVT GmbH, Consolar Solare Energiesysteme GmbH and Splus2 GmbH for their support. The responsibility for the content of this publication lies solely with the authors.

9. References

Brötje, S., Kirchner, M., Schabbach, T. and Giovannetti, F., 2018. Performance Assessment of a Photovoltaic-Thermal Roof with Modular Heat Exchanger, EuroSun 2018 Conference Proceedings, Rapperswil, Switzerland, International Solar Energy Society. DOI: 10.18086/eurosun2018.02.10.

Eurostat, 2023. Shedding light on energy in the EU. Interactive publication, Luxemburg, Eurostat [Online]. DOI: 10.2785/405482.

Gehlin, S. and Spitler, J. D., 2022. Annex 52 - IEA HPT - Long-term performance monitoring of GSHP systems for commercial, institutional, and multi-family buildings, Final report, Heat Pump Centre, Borås, Sweden. DOI: 10.23697/XSBR-XN83.

ISO 9806, 2013. Solar energy — Solar thermal collectors — Test methods, ISO.

Malenković, I., Pärisch, P., Eicher, S., Bony, J. and Hartl, M., 2013. Definition of Main System Boundaries and Performance Figures for Reporting on SHP Systems: Deliverable B1, IEA Solar Heating & Cooling Programme.

Helmling, S., H., Langner, R. and Geimer, K., 2022. Betriebsanalyse von 5 PVT-Wärmepumpensystemen auf Basis von Feldmessdaten über 12 Monate im Rahmen des Projektes integraTE, Tagungsunterlagen: 32. Symposium Solarthermie und regenerative Wärmesysteme, Bad Staffelstein, Germany, 138–152.

Umwelt Bundesamt (2023) Energieverbrauch für fossile und erneuerbare Wärme [Online]. Available at https://www.umweltbundesamt.de/daten/energie/energieverbrauch-fuer-fossile-erneuerbare-waerme accessed 27 July 2023.

Weiss, W. and Spörk-Dür, M., 2023. Solar Heat Worldwide: Global Market Development and Trends 2022, Detailed Market Figures 2021, IEA Solar Heating & Cooling Programme. DOI: 10.18777/ieashc-shw-2022-0001.

Zenhäusern, D., Bamberger, E. and Baggenstos, A., 2017. Energiesysteme mit Photovoltaisch-Thermischen Solarkollektoren, Schlussbericht PVT Wrap-Up, Institut für Solartechnik SPF, HSR Hochschule für Technik Rapperswil, Switzerland.

Giovannetti, F., Lampe, C., Kirchner, M., Littwin, M., Asenbeck, S. and Stephan, F., 2019. Experimental investigations on Photovoltaic-Thermal arrays designed for the use as heat pump source, Santiago, Chile, ISES SWC 2019.